A HIGH-RESOLUTION MAP OF THE COSMIC MICROWAVE BACKGROUND AROUND THE NORTH CELESTIAL POLE[1]

Max Tegmark[1,2,3], Angélica de Oliveira-Costa[2,3,4], Marc. J. Devlin[4], C. Barth Netterfield[4], Lyman Page[4] & E. J. Wollack[4]

[1] *Max-Planck-Institut für Physik, Föhringer Ring 6,D-80805 München*

[2] *Max-Planck-Institut für Astrophysik, Karl-Schwarzschild-Str. 1, D-85740 Garching; angelica@mpa-garching.mpg.de*

[3] *Institute for Advanced Study, Olden Lane, Princeton, NJ 08540; max@ias.edu*

[4] *Princeton University, Department of Physics, Jadwin Hall, Princeton, NJ 08544; page@pupgg.princeton.edu*

Abstract

We present a Wiener filtered map of the Cosmic Microwave Background (CMB) fluctuations in a cap with 15° diameter, centered at the North Celestial Pole. The map is based on the 1993-1995 data from the Saskatoon (SK) experiment, with an angular resolution around 1° in the frequency range 27.6–44.1 GHz. The signal-to-noise ratio in the map is of order two, and some individual hot and cold spots are significant at the 5σ-level. The spatial features are found to be consistent from year to year, reenforcing the conclusion that the SK results are not dominated by residual atmospheric contamination or other non-celestial signals.

[1]Published in *ApJ Letters*, **474**, L77. Available from *h t t p://www.mpa-garching.mpg.de/˜max/saskmap.html* (faster from Europe) and from *h t t p://www.sns.ias.edu/˜max/saskmap.html* (faster from the US). Note that the figures will print in color if your printer supports it.

1 INTRODUCTION

Since the fluctuations in the Cosmic Microwave Background (CMB) depend on a large number of cosmological parameters (see Hu, Sugiyama & Silk 1996 for a recent review), accurate CMB measurements could enable us to measure parameters such as the Hubble constant, the density parameter Ω, *etc.* to hitherto unprecedented accuracy (Jungman *et al.* 1996). After the successful measurements of large-scale fluctuations by COBE team (Smoot *et al.* 1992; Bennett *et al.* 1996), attention is now shifting towards measurements at higher angular resolution.

When reducing a CMB data set, one usually wants to produce either an estimate of the angular power spectrum C_l or a map. Although it is the former that is ultimately used to constrain cosmological parameters, there are a number of reasons for why map making is useful as well (apart from a general desire to map the sky in as many frequency bands as possible):

- It facilitates comparison with other experiments.
- It facilitates comparison with foreground templates such as the DIRBE maps.
- It may reveal flaws in the model that are not visible in the power spectrum, such as non-Gaussian CMB features, point sources and spatially localized systematic problems.

The first degree-scale map reconstructed from difference measurements was produced by White & Bunn (1995) using data from the MAX experiment, which probed a strip of sky a few degrees wide at a resolution of half a degree. The purpose of this *Letter* is to present a map based on data from the Saskatoon (SK) experiment (Wollack *et al.* 1996; Netterfield *et al.* 1997, hereafter "N97"). This map covers a larger patch of sky: a cap of $15°$ diameter centered on the North Celestial Pole (NCP). The angular resolution is similar to that of MAX (about half a degree for the SK95 data), but the region in question is more evenly sampled than was the case with the MAX map, with no "holes".

The map-making method we employ is described in Section 2 and the results are presented and discussed in Section 3.

2 METHOD

The task of generating maps from the Saskatoon data is complicated by the fact that the data set does not contain simple sky temperatures, but rather

2590 different linear combinations of sky temperatures[2]. The i^{th} data point, which we denote y_i, is a linear combination of the temperature across the sky, where the weights ascribed to each patch of sky are given by some known function $f_i(\widehat{\mathbf{r}})$. These weight functions are described in detail in N97. For illustration, four sample weight functions are shown in Figure 1. All weight functions emanate approximately radially from the NCP, oscillate in the radial direction, cover only a small RA-band, and extend to about $8°$ from the pole. The rest of this section describes the inversion process of reconstructing a map from these linear combinations y_i.

2.1 Wiener filtering

Wiener filtering is a general method for estimating a signal from noisy data (Wiener 1949), and can be derived as follows.[3] Suppose that we have a vector of n data points $\mathbf{y}$ and wish to estimate a vector of m numbers $\mathbf{x}$ (for instance the pixel temperatures in a map) from it. Without loss of generality, we can assume that both vectors have zero mean, *i.e.*, $\langle\mathbf{x}\rangle = 0$ and $\langle\mathbf{y}\rangle = 0$, since otherwise, we could redefine them so that they do. Denoting the estimate of $\mathbf{x}$ by $\tilde{\mathbf{x}}$, the most general linear estimate can clearly be written as

$$\tilde{\mathbf{x}} \equiv \mathbf{W}\mathbf{y} \tag{1}$$

for some $m \times n$ matrix $\mathbf{W}$. Defining the error vector as $\varepsilon \equiv \tilde{\mathbf{x}} - \mathbf{x}$, a natural measure of the errors is the quantity $|\varepsilon|$, which is just m times the r.m.s. error per data point. The expectation value of $|\varepsilon|^2$ is given by

$$\langle|\varepsilon|^2\rangle = \langle(\mathbf{W}\mathbf{y}-\mathbf{x})^t(\mathbf{W}\mathbf{y}-\mathbf{x})\rangle = \mathrm{tr}\left[\mathbf{W}\langle\mathbf{y}\mathbf{y}^t\rangle\mathbf{W}^t - 2\langle\mathbf{x}\mathbf{y}^t\rangle\mathbf{W}^t + \langle\mathbf{x}\mathbf{x}^t\rangle\right]. \tag{2}$$

The Wiener filter $\mathbf{W}$ is the matrix that minimizes this error. [4] By differentiating with respect to the components of $\mathbf{W}$, we obtain the simple result

$$\mathbf{W} = \langle\mathbf{x}\mathbf{y}^t\rangle\langle\mathbf{y}\mathbf{y}^t\rangle^{-1}. \tag{3}$$

[2] The present analysis is based on the CAP data (as defined in N97) and does not include the RING data.

[3] If the data set is Gaussian, an alternative derivation the Wiener filter is to maximize the a posteriori probability distribution, *i.e.*, to find the most likely map given the data (Zaroubi *et al.* 1995).

[4] Since the reconstruction of pixel i depends only on the i^{th} row of $\mathbf{W}$, this is equivalent to minimizing all the errors ε_i^2 separately.

Direct substitution shows that the covariance matrix of the estimates is

$$\langle\tilde{\mathbf{x}}\tilde{\mathbf{x}}^t\rangle = \langle\mathbf{x}\mathbf{y}^t\rangle\langle\mathbf{y}\mathbf{y}^t\rangle^{-1}\langle\mathbf{y}\mathbf{x}^t\rangle \tag{4}$$

and that the error covariance matrix is

$$\langle\varepsilon\varepsilon^t\rangle = \langle\mathbf{x}\mathbf{x}^t\rangle - \langle\mathbf{x}\mathbf{y}^t\rangle\langle\mathbf{y}\mathbf{y}^t\rangle^{-1}\langle\mathbf{y}\mathbf{x}^t\rangle. \tag{5}$$

Linear filtering techniques have recently been applied to a range of cosmological problems. Rybicki & Press (1992) give a detailed discussion of the one-dimensional problem. Lahav *et al.* (1994), Fisher *et al.* (1995) and Zaroubi *et al.* (1995) apply Wiener filtering to galaxy surveys. The COBE DMR maps have been processed both with Wiener filtering (Bunn *et al.* 1994; Bunn *et al.* 1996) and with other linear filtering techniques (Bond 1995).

2.2 Application to the Saskatoon case

In our case, the observed data point y_i is the true sky temperature distribution $x(\widehat{\mathbf{r}})$ convolved with the i^{th} beam function $f_i(\widehat{\mathbf{r}})$, with noise n_i added afterwards, so

$$y_i = n_i + \int f_i(\widehat{\mathbf{r}})x(\widehat{\mathbf{r}})d\Omega. \tag{6}$$

Our maps will cover a square region of $20^\circ \times 20^\circ$ centered on the NCP, pixelized into a 64×64 square grid, so $m = 4096$. To ensure that the maps are properly oversampled, we define the pixels to be the sky temperatures after Gaussian smoothing on a scale of $\sigma = 1^\circ$:

$$x_i = \int \phi(\widehat{\mathbf{r}}_i\cdot\widehat{\mathbf{r}})x(\widehat{\mathbf{r}})d\Omega, \tag{7}$$

where $\widehat{\mathbf{r}}_i$ is a unit vector in the direction of the i^{th} pixel and

$$\phi(\cos\theta) \equiv \frac{1}{2\pi\sigma^2}e^{-\theta^2/2\sigma^2}. \tag{8}$$

This means that the map resolution σ is 3.2 times the pixel separation $20^\circ/64$, which is safely above the Shannon oversampling rate of 2.5. In order to apply the Wiener filtering procedure, we need to compute the matrices $\langle\mathbf{y}\mathbf{y}^t\rangle$ and $\langle\mathbf{x}\mathbf{y}^t\rangle$. The former contains the correlation between the data points and themselves, and is given by

$$\langle y_i y_j\rangle = \langle n_i n_j\rangle + \int\int f_i(\widehat{\mathbf{r}})f_j(\widehat{\mathbf{r}}')c(\widehat{\mathbf{r}}\cdot\widehat{\mathbf{r}}')d\Omega d\Omega', \tag{9}$$

where the correlation function c is given by the angular power spectrum C_l through the familiar relation

$$c(\cos\theta) = \sum_{l=0}^{\infty}\left(\frac{2l+1}{4\pi}\right)P_l(\cos\theta)C_l, \tag{10}$$

where $\mathbf{P}_l$ are the Legendre polynomials. As described in N97, the noise covariance matrix $\langle\mathbf{n}\mathbf{n}^t\rangle$ is almost diagonal for the Saskatoon experiment, but there are a small number of non-zero correlations (for example, there is a 2% anticorrelation between the Ka94 5pt East data and the simultaneously acquired Ka94 7pt East data due to mainly to atmospheric noise).

Likewise, the correlation between the data points and the pixels is given by

$$\langle x_i y_j\rangle = \int\int\phi(\widehat{\mathbf{r}}_i\cdot\widehat{\mathbf{r}}')f_j(\widehat{\mathbf{r}})c(\widehat{\mathbf{r}}\cdot\widehat{\mathbf{r}}')d\Omega d\Omega'. \tag{11}$$

2.3 Practical Issues

To compute the covariance matrices $\langle\mathbf{x}\mathbf{y}^t\rangle$ and $\langle\mathbf{y}\mathbf{y}^t\rangle$, we approximate the integrals in equations (9) and (11) by sums over a 256×265 grid of points. Direct computation of $\langle\mathbf{y}\mathbf{y}^t\rangle$ with this procedure would take over a decade on a typical workstation, even if the code were optimized by omitting from the double sum all pixels where f_i or f_j are zero. Fortunately, the relevant angular separations are all much less the a radian, which means that the effect of sky curvature is negligible. To a good approximation, we can thus integrate over a flat two-dimensional plane instead and obtain

$$\langle\mathbf{y}\mathbf{y}^t\rangle-\langle\mathbf{n}\mathbf{n}^t\rangle\approx\int\int f_i(\mathbf{r})f_j(\mathbf{r}')c(\mathbf{r}-\mathbf{r}')d^2r d^2r' = \int\int f_i(\mathbf{r})(f_j\star c)(\mathbf{r})d^2r, \tag{12}$$

where $\star$ denotes convolution. Using fast Fourier transforms (FFTs) to compute the convolutions, the entire covariance matrix can now be computed in merely a day. The computation of $\langle\mathbf{x}\mathbf{y}^t\rangle$ can be accelerated in the same way.

Because the electronic offset is unknown, the means must be removed from the observations with each of the 64 synthesized beam patterns, which corresponds to multiplying the data vector $\mathbf{y}$ by a certain projection matrix $\mathbf{P}$. We thus use the corrected covariance matrices $\langle\mathbf{x}\mathbf{y}^t\rangle\mathbf{P}^t$ and $\mathbf{P}\langle\mathbf{y}\mathbf{y}^t\rangle\mathbf{P}^t$ in place of $\langle\mathbf{x}\mathbf{y}^t\rangle$ and $\langle\mathbf{y}\mathbf{y}^t\rangle$ in equation (3). We find that this correction makes a difference of only a few percent.

3 RESULTS AND CONCLUSIONS

The resulting map is shown in Figure 2 (bottom right) and in Figure 3. The fiducial power spectrum used is described in section 3.2 below. As expected, it contains virtually no features more than 8° from the center, reflecting the fact that the sky outside of this circle was not probed by any of the beam functions. Computation of the relevant covariance matrices shows that the signal-to-noise ratio within this disc is fairly constant and of order two. In other words, the main features visible in this map are expected to be real rather than mere noise fluctuations. We also generated a number of mock Saskatoon data sets, ran them through the inversion software and compared the reconstructions with the original maps, which confirmed this conclusion.

3.1 Comparison between Years

The three first panels in Figure 2 show maps generated from the subsets of the data that were taken in 1993, 1994 and 1995, respectively. The 1993 data is seen to be rather featureless, reflecting the fact that the 1993 data set (42 data points) contains considerably less information than the other two years of data. Similarly, the 1995 map is seen to contain more small-scale structure than the 1994 map, reflecting the fact that the angular resolution was approximately doubled in 1995. Most potential sources of problems with the experiment (underestimation of atmospheric contamination, sidelobe pickup from celestial bodies, *etc.*) would be expected to vary on timescales much shorter than a year. In addition, the beam patterns were quite different in the three years as described in N97 – for instance, the beam width was substantially reduced in 1995 as mentioned above. The visual similarity between these independent maps therefore provides reassuring evidence that the bulk of the signal being detected is in fact due to temperature-fluctuations on the sky rather than unknown systematic problems.

In addition to a qualitative visual inspection, the 1994 and 1995 maps can be used to make more quantitative consistency checks. For example, we subtracted one from the other and compared the resulting noise levels with the theoretical expectations (as given by the diagonal of $W\langle\mathbf{nn}^t\rangle W^t$). The levels are in good agreement, indicating that there is no evidence for additional unmodeled/overlooked sources of noise.

The perhaps most striking single feature in the maps, which stands out in all three years of data, is the large cold spot around "two o'clock", about half way from the center. It is interesting to note that the existence of this cold spot can be qualitatively inferred from the plots of the raw data in Wollack *et al.* (1993) and Netterfield *et al.* (1994), since the three-point beam (which has a positive lobe half-way from the center) was found to give large negative temperature between 4 and 5 hours in RA.

3.2 Dependence on method details

To test if the reconstructed map is sensitive to the pixel size, the analysis was repeated with 32×32 pixels. As expected, this produced virtually identical maps, since the original 64×64 pixel map was substantially oversampled.

The maps in Figure 2 where generated using a a featureless (flat) fiducial power spectrum $C_l = 6Q^2/l(l+1)$ normalized to $Q = 20\mu$K. To what extent do the maps depend on this choice? As described below, the short answer to this question is "almost not at all". As a test, we repeated the analysis for flat power spectra with $Q = 0$, 10μK, 47μK (the best fit to the Saskatoon power spectrum points of N97) and 60μK, as well as for four different normalizations of the standard CDM models (Sugiyama 1995). The spatial features remained essentially unchanged, and the different normalizations simply caused different degrees of smoothing. The appearance of the map depended essentially only on one single property of the power spectrum: the broad-band power on the angular scales where the SK experiment is sensitive. This behavior is easy to understand from equation (3). Note that whereas $\langle \mathbf{y}\mathbf{y}^t \rangle$ is a sum of two contributions, one from signal and one from noise, $\langle \mathbf{x}\mathbf{y}^t \rangle$ depends only on the signal. Roughly speaking, $\mathbf{W}$ is thus of the form signal/(signal+noise). In the extreme case of no signal ($Q = 0$), the Wiener-filtered map thus becomes identically zero, since $\langle \mathbf{x}\mathbf{y}^t \rangle = 0$. If we increase the assumed signal-to-noise ratio, generic components of $\mathbf{W}$ increase in magnitude, and the Wiener filtering process will attempt to recover more details in the map. Since the noise loosely speaking enters on smaller scales than the signal, assuming a lower signal-to-noise ratio will basically cause the filtering to suppress high frequencies more than low frequencies, *i.e.*, smooth the map more. In summary, using a fiducial power spectrum with the wrong amount of power in the SK band will produce a map with the same spatial features in the same locations, but simply smoothed either more or less than what is optimal.

Which is the best fiducial power level to use? The answer to this question depends on our desired signal-to-noise ratio S/N (which we define as the ratio of the r.m.s. signal and the r.m.s. noise). The variance in a map pixel is given by the corresponding diagonal element of $W\langle \mathbf{y}\mathbf{y}^t \rangle W^t$, so we can separate the contributions of signal and noise by splitting $\langle \mathbf{y}\mathbf{y}^t \rangle$ into a signal and a noise part and then compute S/N. Since the Wiener filtering balances between smoothing too little (getting swamped by noise) and smoothing too much (loosing unnecessarily much of the small-scale signal), it typically produces a map where these two problems are comparable in magnitude, *i.e.*, where the noise is comparable to the *lost* part of the signal. Since S/N compares the noise to the part of the signal which was *not* lost, there is no a priori guarantee that the S/N obtained will be satisfactory. It is thus common to adjust the fiducial power level to obtain a desired S/N. In our case, $S/N \approx 1.3$ for the combined map when the fiducial band power was $Q = 47\mu$K, so we chose $Q = 20\mu$K to get a more smoothed and less noisy map, which has $S/N \approx 2.0$.

By dividing the map by the r.m.s. noise σ, we can read off the significance level of individual map features. [5] For instance, the cold spot around "two o'clock" is -7σ, the one at "eight o'clock" is -5σ and the hot spot at "ten o'clock", near the center, is $+5\sigma$.

In conclusion, we have presented the largest map to date of the CMB at degree scale angular resolution. The signal-to-noise ratio is of order two, and some individual hot and cold spots are significant at the 5σ level. It is hoped that this map can be used to make comparisons between experiments and with various foreground templates, thereby improving our understanding of systematics and foregrounds in preparation for the next generation of CMB missions.

The authors wish to thank David Wilkinson for helpful comments on the manuscript. Support for this work was provided by NASA through a Hubble Fellowship, HF-01084.01-96A, awarded by the Space Telescope Science Institute, which is operated by AURA, Inc. under NASA contract NAS5-26555, by European Union contract CHRX-CT93-0120, by Deutsche Forschungsgemeinschaft grant SFB-375, by NSF grant PH 89-21378, NASA grants NAGW-2801 and NAGW-1482, a Cottrell Scholar Award of Research Corp, a David Lucile Packard Foundation Fellowship, and an NSF NII grant to L. Page.

[5] More generally, equation (5) can be used to place error bars on linear combinations of map pixels (such as correlations with external templates) and to make so-called constrained realizations (see *e.g.* Zaroubi *et al.* 1995).

4 REFERENCES

Bennett, C. L. 1996, *ApJ*, **464**, L1.

Bond, J. R. 1995, *Phys. Rev. Lett.*, **74**, 4369.

Bunn, E. F. *et al.* 1994, *ApJ*, **432**, L75.

Bunn, E. F., Hoffmann, Y & Silk, J 1996, *ApJ*, **464**, 1.

Fisher, K. B. *et al.* 1995, *MNRAS*, **272**, 885.

Hu, W., Sugiyama, N. & Silk, J. 1996, preprint astro-ph/9604166.

Jungman, G.. Kamionkowski, M., Kosowsky, A & Spergel, D. N. 1996, *Phys. Rev. D*, **54**, 1332.

Lahav, O. *et al.* 1994, *ApJ*, **423**, L93.

Netterfield *et al.* 1995, *ApJ*, **445**, L69.

Netterfield, C. B. *et al.* 1997, *ApJ*, **474**, 47.

Rybicki, G. B. & Press, W. H. 1992, *ApJ*, **398**, 169.

Smoot, G. F. *et al.* 1992, *ApJ*, **396**, L1.

Sugiyama, N. 1995, *ApJS*, **100**, 281.

White, M. & Bunn, E.F. 1995, *ApJ*, **443**, L53.

Wiener, N. 1949, *Extrapolation and Smoothing of Stationary Time Series* (NY: Wiley).

Wollack, E. J. *et al.* 1993, *ApJ*, **419**, L49.

Wollack, E. J. *et al.* 1996, preprint astro-ph/9601196.

Zaroubi, S. *et al.* 1995, *ApJ*, **449**, 446.

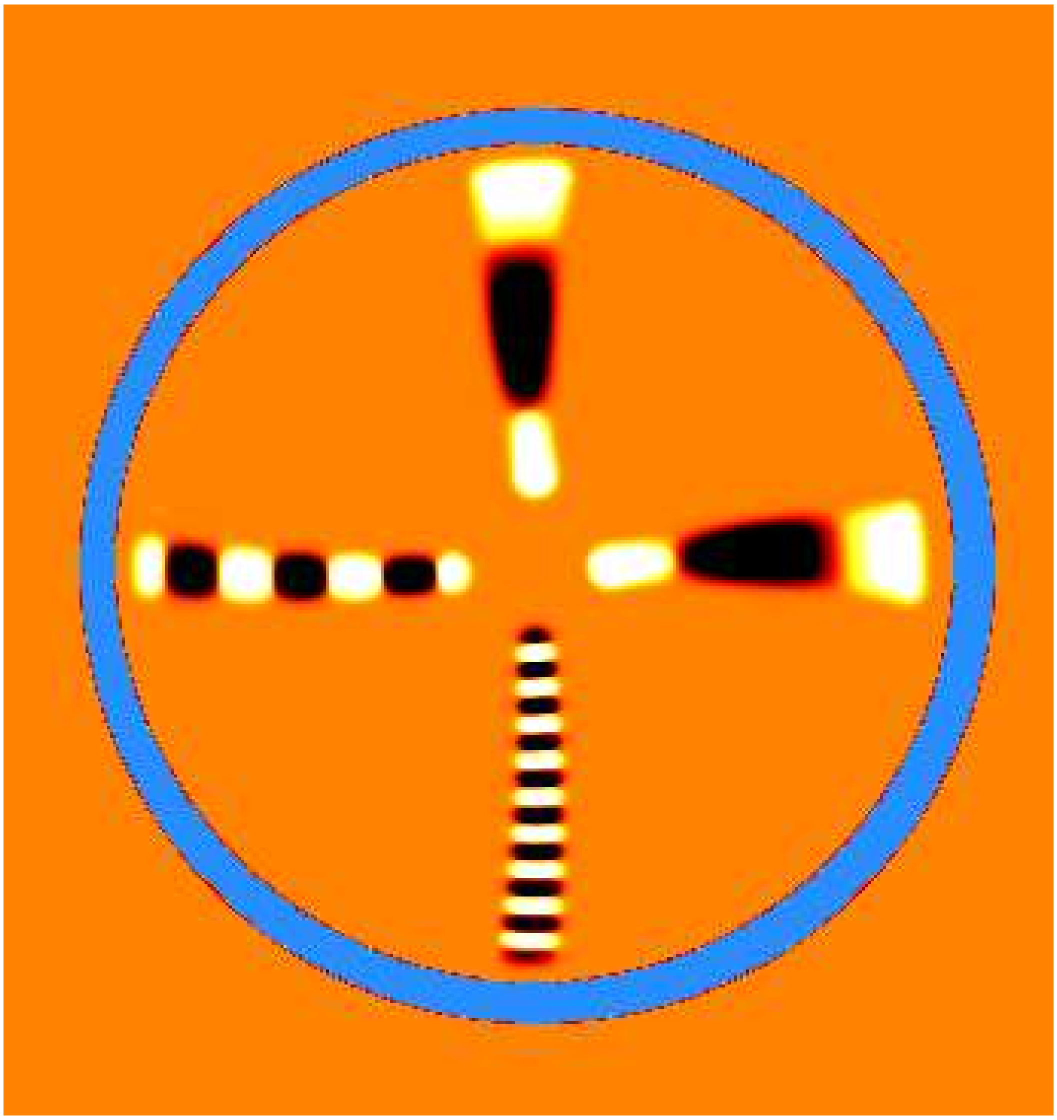

Figure 1: Sample Saskatoon weight functions.
Four of the 2590 Saskatoon weight functions are shown in a circle of diameter $16°$ with the North Celestial Pole at the center. The weight functions are all for the 1995 East data, and correspond to the 3-point beam in the RA =0h azimuthal bin (top), the same beam in the RA =6h azimuthal bin (right), the 19-point beam in the RA =12h azimuthal bin (bottom) and the 7-point beam in the RA =18h azimuthal bin (left).

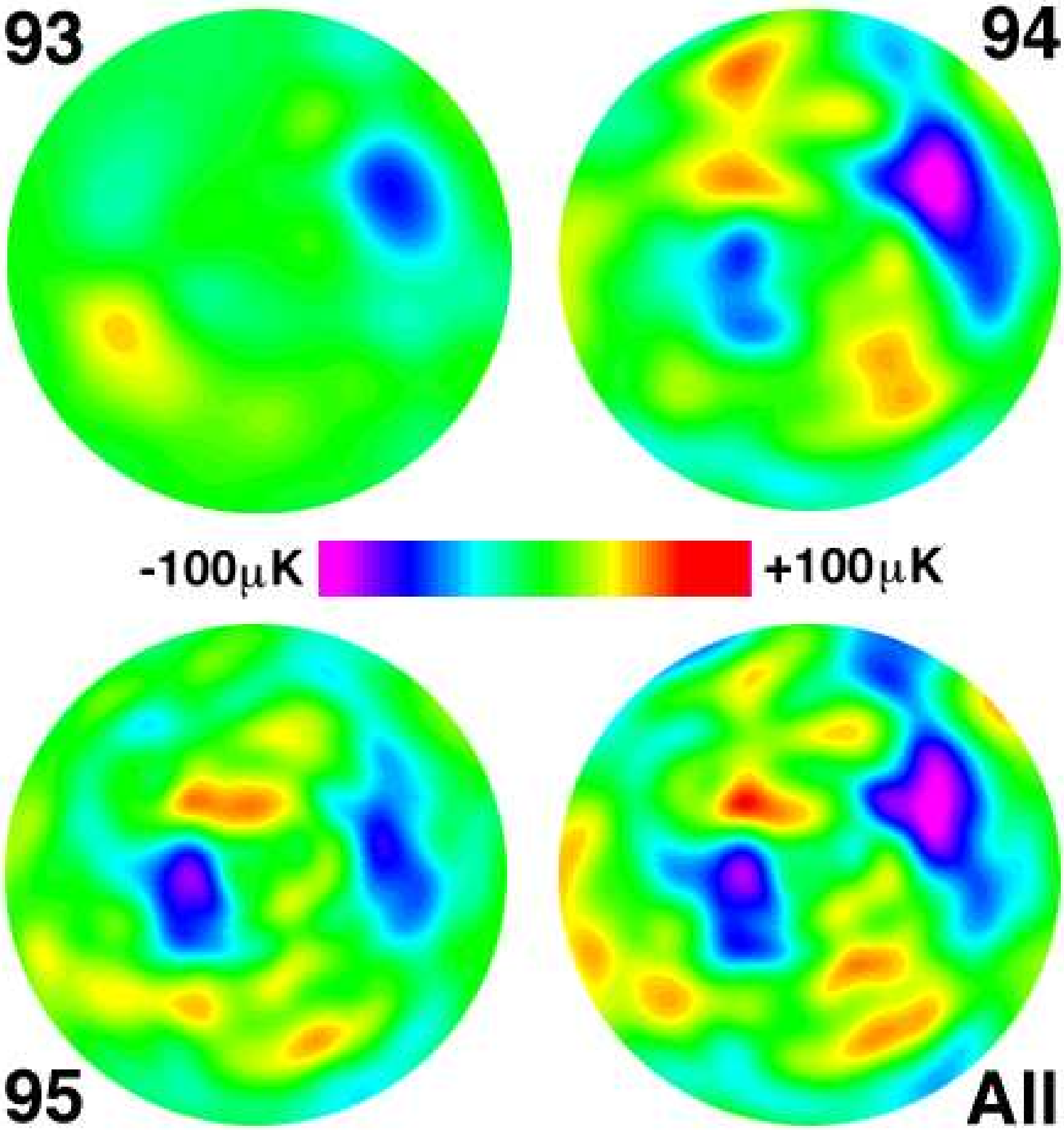

Figure 2: Wiener-filtered maps.

The CMB temperature is shown in coordinates where the North Celestial Pole is at the center of a circle of 16° diameter, with RA being zero at the top and increasing clockwise. The first three panels show the maps using only the 1993, 1994 and 1995 data sets, respectively. The last panel (bottom right) shows the map based on all three years of data.

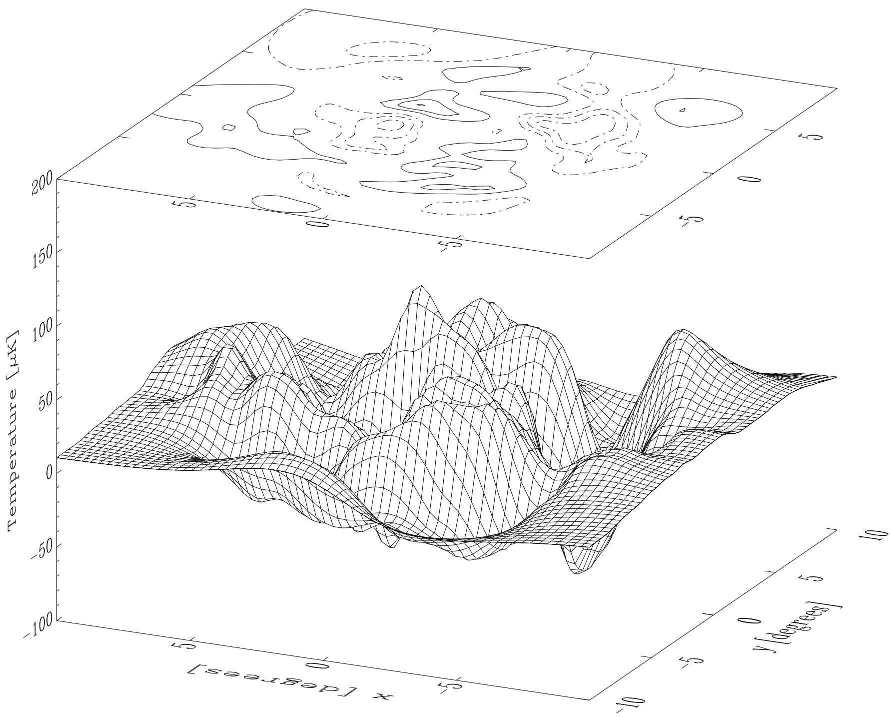

Figure 3: The Wiener-filtered map.
The map based on the entire data set (bottom right in Figure 2) is shown in coordinates where the North Celestial Pole is at the center of a $20° \times 20°$ square with RA being zero at the top and increasing clockwise. $RA = 0$ is at $(x, y) = (0, 10°)$. The contour curves correspond to -75μK, -50μK, -25μK, 25μK, 50μK and 75μK, respectively.